Chapter IV Result and Discussion

4.1 Integration of CNTs and AAO

4.1.1Microstructure of AAO template

Figs. 4-1(a)-(c) are the inch by inch charts of fabricating nanoporous AAO film by two-step anodization and theirs corresponding SEM images. Fig. 4-1(a) demonstrates that the nanopores in disorder are formed in the first anodiztion step but it shows a roughly distribution along with the direction of stress within the Al film. After wet chemical etching at 60 °C with a mixed solution of H_3PO_4 and CrO_3, the ordered pre-structured surface of Al is obtained in Fig. 4-1(b). Comparing fig. 4-1(a) with (b), it is clear that the pore nucleation sites on Al surface are random and gradually merge to a significant size. This result is the same with previous reports.[Li-1998-2470][Li-1998-6023] Finally, ordered nanoporous arrays are accomplished with the following secondary anodization [Fig. 4-1(c)].

The curve of current density changes versus anodization time and corresponding schemas are shown in Fig. 4-2 (a) & (b), respectively. It can be separated into four stages of the process approximately. At stage Ⅰ, a barrier oxide layer begins to grow on surface of aluminum causing the current density decrease rapidly. And relatively fine-featured pathway are then revealed during stage Ⅱ. After this, the current density starts to raise because the individual paths through the barrier oxide with their heads become enlarged in stage Ⅲ. It

increase continuously until the reaction reaches steady-state. In stage Ⅳ, the pore growth turns stable, and pore structure is formed by closely packed cylindrical cells.

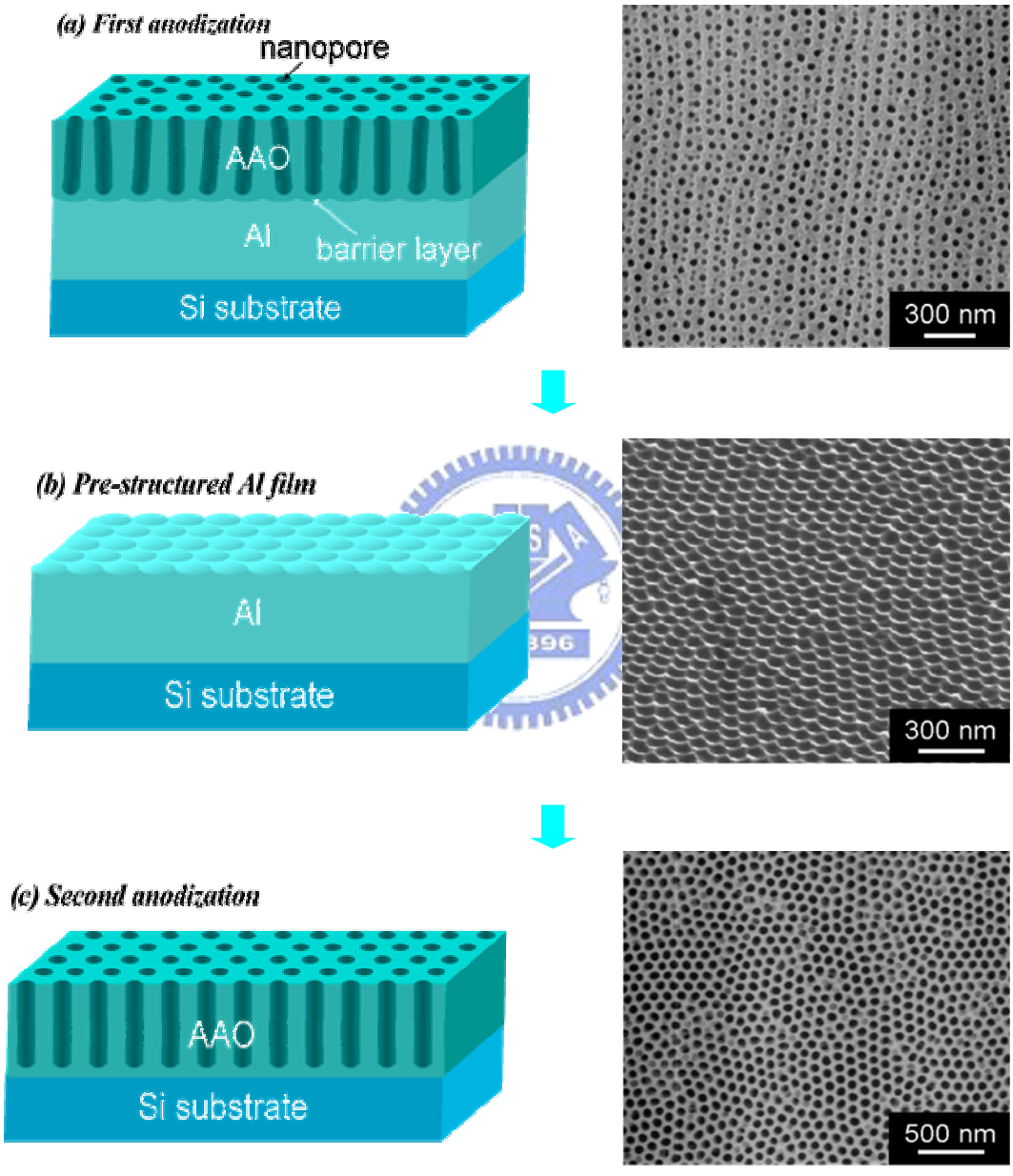

Figs. 4-1(a)(b)(c). Inch by inch charts of fabricating nanoporous AAO film by two-step anodization and corresponding SEM images.

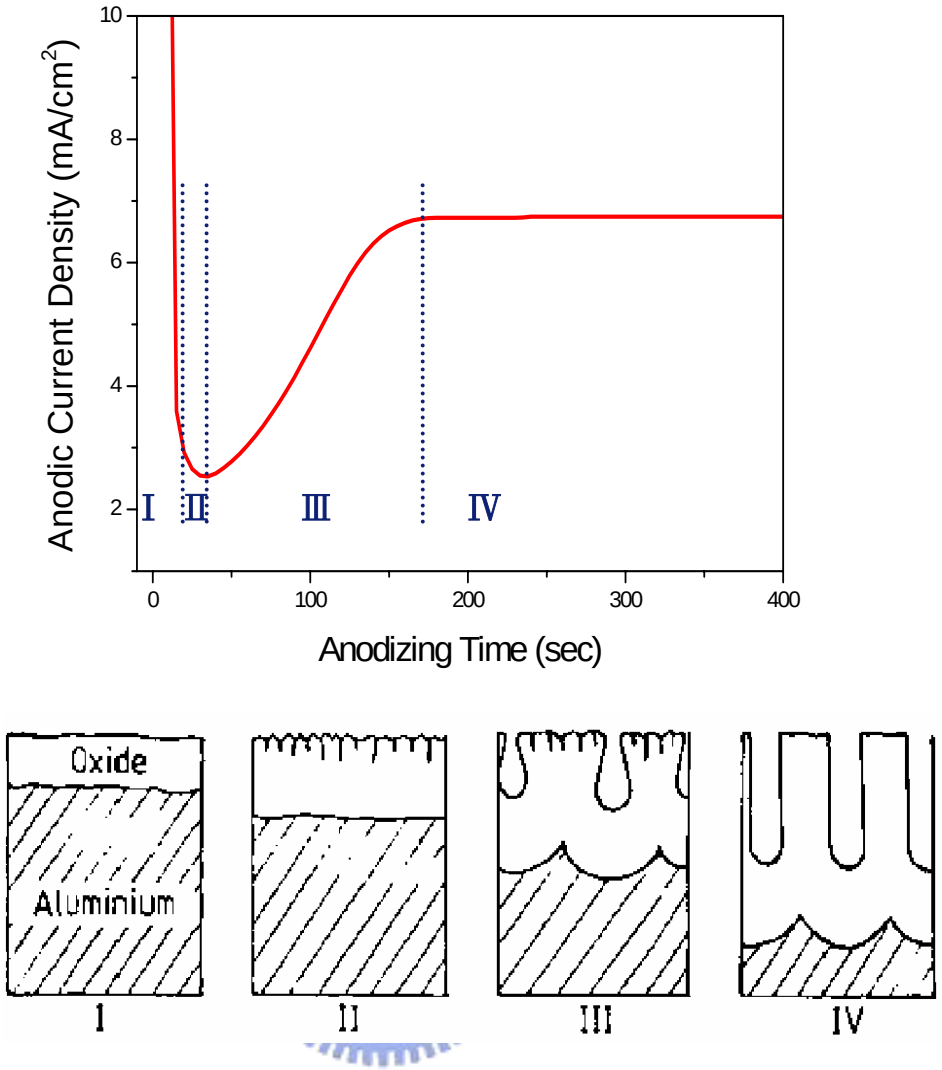

Fig. 4-2. Current density variety and corresponding schemas during aluminum anodization.

Fig. 4-3 shows the top-view SEM micrographs of the nanoporous AAO film after the two-step anodization and pore widening under the same conditions as those in Fig. 4-1. The self-organized nanopores with a uniform size distribution have a pore diameter about 60 nm and an interpore distance about 100 nm. The AAO nanopores do not show a long-range ordering, but within a pore array domain, ordered nanopore with a hexagonal arrangement is clearly observed.

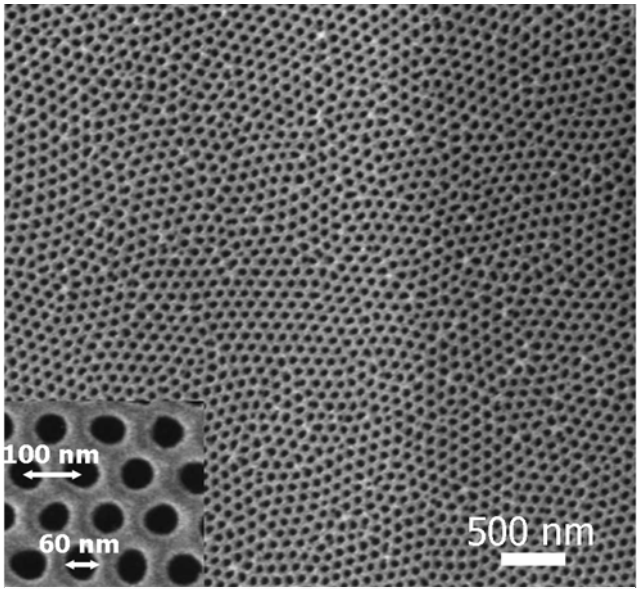

Fig. 4-3. Top-view SEM image of the nanoporous AAO film after pore widening in a H_3PO_4 solution for 60 min. The inset shows close-up view of AAO nanopores.

Because of volume expansion during Al anodization, stresses are formed at the interface of aluminum and alumina. In order to study stresses effect of ordered domain, relative ratio of the thickness of alumina layer and the aluminum layer consumed has been examined. The volume expansion factor can be changed quite dramatically from about 0.8 up to 1.7 by varying the experimental anodization parameters. In the experiment, the factor is about 1.4. This result exactly conforms to a report proposed by Li et al. [Li-1998-6023] in 1998. They utilized three types of most popular acids, i.e. sulfuric, oxalic, phosphoric, to practice Al anodization. After a series of tests and calculations, a moderate value 1.4

of volume expansion was obtain for ordered pore arrangements. Moreover, the size of ordered domain which is about 0.25-1.0 μm^2 can also be measured from fig. 4-3. This value resembles the result proposed by Li et al..[Li-1998-2470] Their research team considered that maybe the bottoms of the pores could move around, and the domains grew by alignments and mergers of pores at domain boundaries, i.e., the domain size was a function of time. This is very similar to grain growth in metals and alloys, and can be described as the empirical equation. For metals and alloys, the driving force of grain growth is the grain boundary energy per unit area. For grain growth at a fixed temperature, the average radius R of the grain is a function of the time t:

$$R = Bt^n \qquad (4\text{-}1)$$

Where B is a temperature-dependent parameter and n is about 0.5-0.4.[Tu-1992-370] As the pores moved and merged, the orientation of adjacent domains could change gradually, so domains smoothly matched. With their experimental data, the ordered domain area was about 0.2-0.5 μm^2 at 15 °C.

Fig. 4-4(a) is the cross-sectional view of the AAO film before Co electroplating. The depth of the straight cylindrical pores is about 740 nm. It is obvious that the insulative alumina barrier layer under each pore bottom was removed completely during the pore widening step. On the other hand, fig. 4-5(b) also shows cross-sectional view of AAO film with the same process conditions ex-

cept the voltage decrease at the end of second anodization. There is a barrier layer about 50nm apparently exist at the each pore bottom. After the Co electroplating uniform catalyst particles were deposited at the AAO pore bottom [Fig. 4-5].

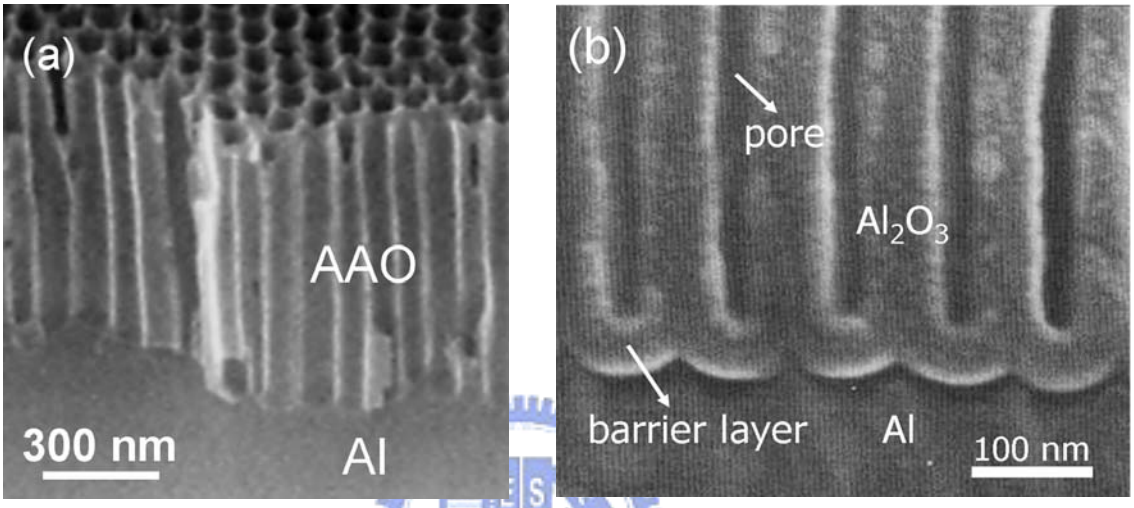

Fig. 4-4. The cross-sectional SEM micrograph of AAO film with barrier layer removal (a), and without barrier layer removal (b).

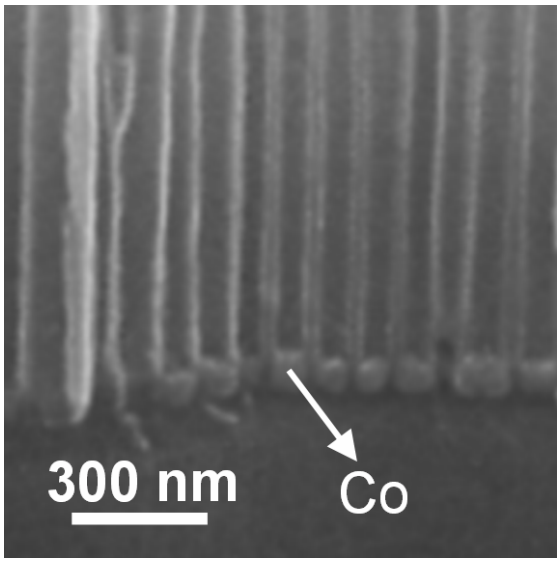

Fig. 4-5. Cross-sectional SEM image of AAO film after electroplating Co catalyst

4.1.2 Microstructure of AAO assisted CNTs

Lee et al. have reported the growth of CNTs in the AAO template with or without deposition of Co in the pore bottom as the catalyst.[Lee-2001-2387] It was suggested that AAO as well as Co catalyst all play an important role on the pyrolysis of hydrocarbon precursors. CNTs were only grown in the pore channels of the AAO template when Co was not present, and these tubes have a very poor crystallinity.[Takashi-1996-2109, Eun-2002-277, Sui-2001-1523] When the Co catalyst was deposited into the pores, both AAO and Co played important role to assist the growth of the CNTs. Because Co is a much more active catalyst for hydrocarbon decomposition,[Jeong-2001-2052] the catalyst role of Co was dominant. The well-graphitized CNTs grew out of the pores due to a high growth rate and entwined above the pores. Fig. 4-6 shows the side-view SEM images of the Co-catalyzed CNTs grown on the AAO template by using the microwave plasma ECR-CVD. Similar to previous works, the CNTs also grew out of the pores as shown in Fig. 4-6, but the tubes aligned vertically to the AAO surface with little entanglement. In the earlier stage of the growth, the template effect of the AAO nanopores constrains the tubes to grow along the axis of the pores, resulting in the growth of the well-aligned tubes. After extending out of the pores, the overgrown CNTs remained the vertical growth direction due to the applied DC bias

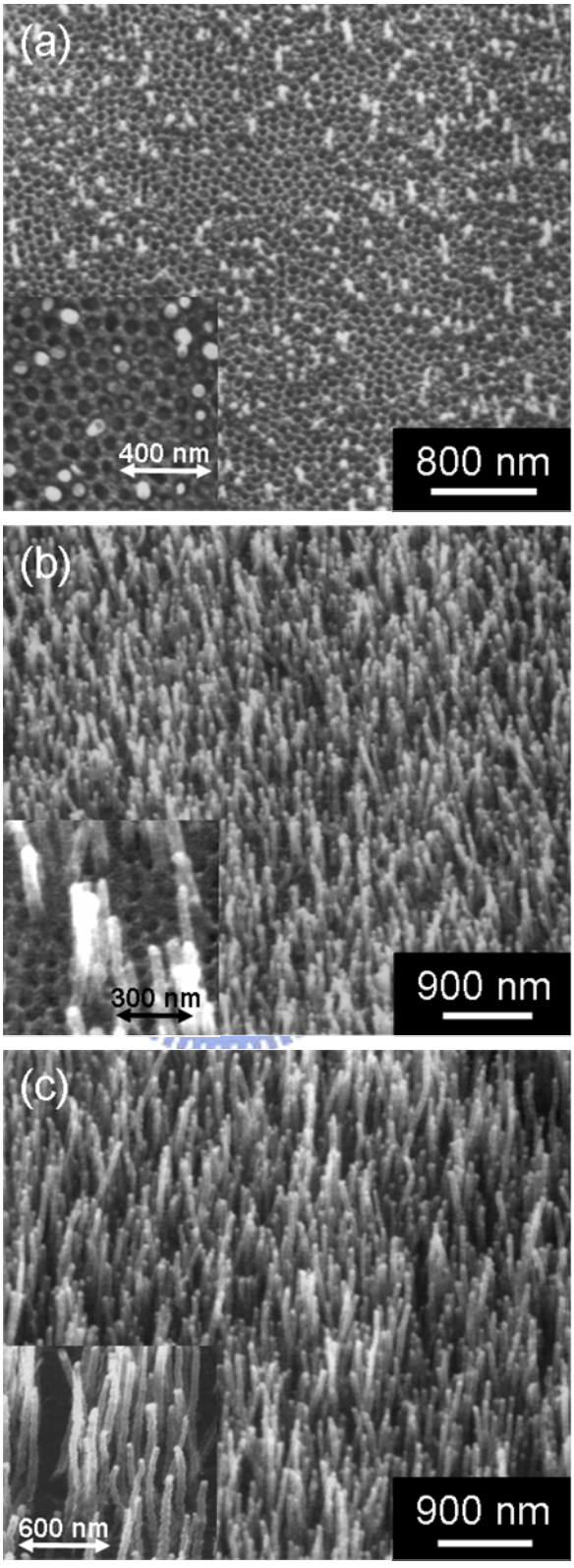

Fig. 4-6. Side-view SEM images of the Co-catalyzed CNTs grown on the AAO template by using the ECR-CVD for (a) 7 min, (b) 15 min, and (c) 30 min. The insets show the close-up view of the CNTs grown out of the AAO template pores.

and the plasma induced electric field (self-bias) in the ECR plasma environment. The electrostatic force would force the exposed CNTs to align with the electric field.[Bower-2000-830] By using the AAO template, the CNTs of a very high packing density (~6×10^9 tubes/cm^2) are highly uniform in diameter with an average of about 75 nm, which is coincided with the pore size of the AAO template. However, the diameter of tubes is lager than that of the AAO pores before the CNT growth shown in Fig. 4-3. This is possibly due to water loss in the AAO template from heating during the CVD process resulting in the enlargement of AAO pores.[Jung-1999-2047]

From Fig. 4-6 it can be clearly seen that the length of the CNTs increases with the growth time. As seen in Fig. 4-6 (a), most of the CNTs are shorter than the depth of pore channels after CNT growth of 7 min, and only a few tubes are observed to extend over the pores. After 15 min growth [Fig. 4-6(b)], it is obvious that the almost all the CNTs grew out of the pores, and the overgrowth length was about 300-700 nm. In the case of growth of 30 min [Fig. 4-6(c)], most of the tubes above the template had a length of 700 nm-1.5 μm. If the growth time was increased further, the tube length would not increase any longer, suggesting the Co catalyst was possibly poisoned. In the fabrication of triode field emitters using CNTs, one of the challenges is to control the length of aligned CNTs in the submicron scale without the overgrowth from the gate

hole.[Lee-2001-479] The growth rate of CNTs in the AAO template by ECR-CVD is considerably low (~60 nm/min), and, therefore, the tube length can be reliably controlled via the growth time. Thus the CNTs are potentially suitable for the field emitter applications.

Fig. 4-7(a) shows a cross-sectional TEM image of the sample shown in Fig. 4-6(b). It is obvious that the Co catalyst particles are encapsulated at the tips of tubes and covered by graphitic caps. Also, there are residual Co at the pore bottom. Fig. 4-7(b) shows a selected-area electron diffraction pattern recorded from the overgrown part of the tubes shown in Fig. 4-7(a). Three diffraction rings can be clearly identified to be (002), (100), and (110) of graphite. The diffraction pattern suggests that the tubes have a graphitic form with an interwall distance (d_{002}) of approximately 3.6 Å, which is larger than the interplanar separation of graphite (d_{002}=3.35 Å). The larger interwall distance results from the curvature of the graphitic walls. Fig. 4-7(c) is a plan-view high-resolution TEM (HRTEM) image showing a CNT inlaid in a pore of the AAO template. Since the tube has a relatively large diameter, only a part of the tube is shown in this figure. The tube is composed of about 70-80 graphitic walls, and the tube size is strongly defined by the AAO pore geometry. Table 4-1 shows the features of CNTs in the experiment.

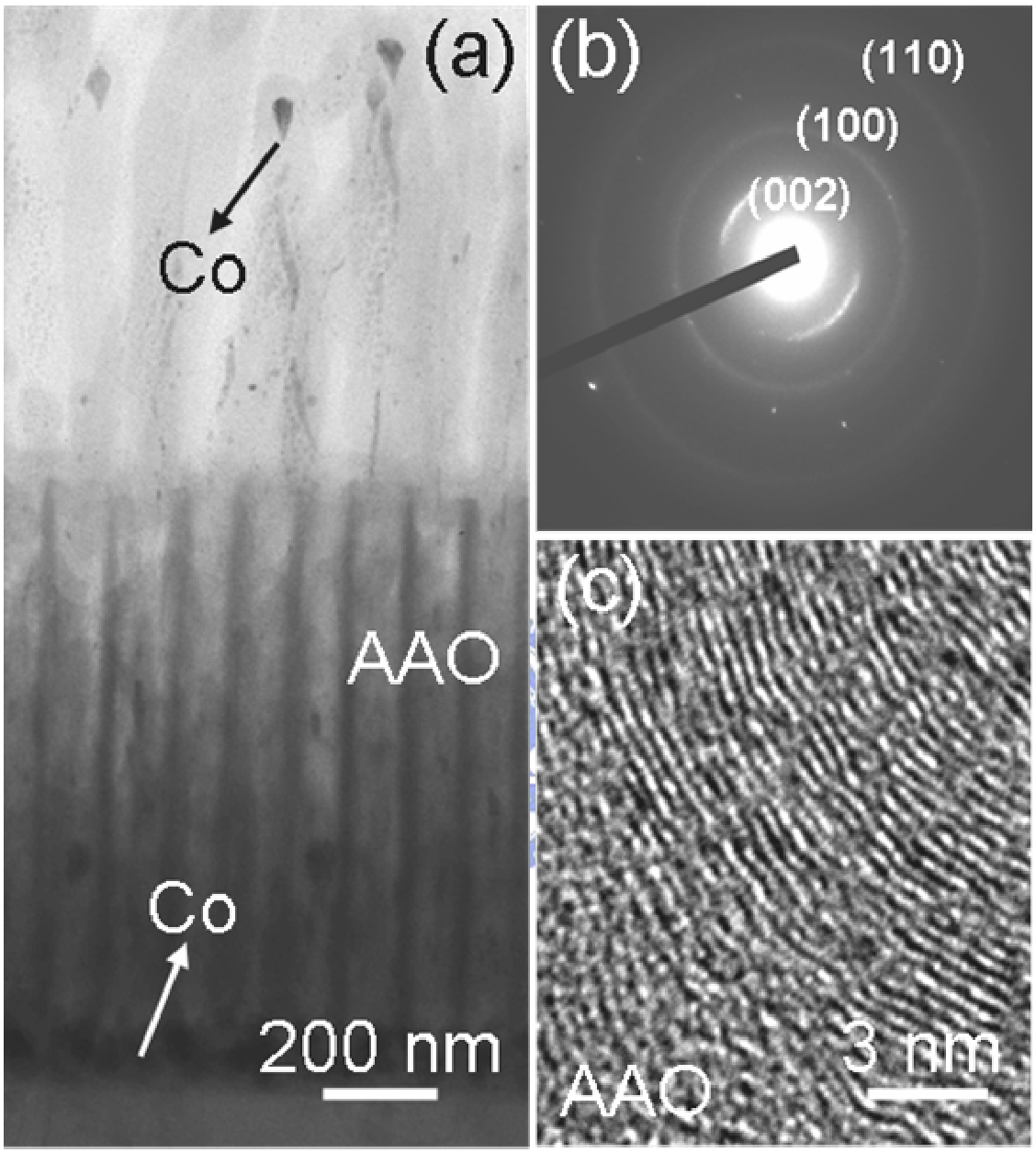

Fig. 4-7. (a) Cross-sectional TEM image of the very sample shown in Fig. 4-6(b). The surface was covered with an amorphous Si film to protect the exposed CNTs. (b) Electron diffraction pattern recorded from the overgrown part of the tubes shown in (a). (c) Plan-view HRTEM image of the walls of a graphitized CNT inlaid in an AAO pore.

Growth time (min)	Overgrown tube length (nm)	Tube Diameter (nm)	Tube number density (tubes/cm2)	No. of Graphene layers
7	< 100	~ 75	~ $7x10^9$	70 ~ 80
15	300 ~700			
30	700 ~1500			

AAO hole density = 1 x 10^{10} pores/cm^2

Pore diameter = ~ 75 nm

Table 4-1. Features of CNTs

4.1.3 Growth Mechanism of CNTs in AAO

The growth mechanism of CNTs prepared by the catalytic decomposition of hydrocarbon vapors has been divided into either tip or base growth.[Baker-1989-315] Although residual Co catalyst can also be observed in the tube base [Fig. 4-7(a)], the growth mechanism of the CNTs tends to be the tip growth rather than base growth for the present case. With regard to the base growth, the precursor gases must continuously transport to the Co catalyst at pore bottom. If the gas diffusion is blocked, the catalytic growth of CNTs will be terminated. However, under the experimental condition, the nanopores are compactly filled with multiwalled CNTs [Fig. 4-7(c)] and, moreover, the tubes have

a closed end [Fig. 4-7(a)]. The encapsulated Co nanoparticles at their tips can block the gas diffusion implying that the base growth is unfavorable. In the tip growth, the gas diffusion will not be obstructed because the CNT growing site is at the tip of the tubes.

It should be noted that the number of the graphitic layers is independent on the growth time, and this is unlike the layer-by-layer growth mechanism proposed by Yao et al.[Yao-2001-11395]. They found that when the AAO was used alone to act as a catalyst to grow CNTs, the thickness of tube walls increased with increasing the growth time, inferring that the graphite was deposited layer-by-layer on the inner wall of the AAO pore. In regard to the Co-catalyzed growth of CNTs, increase of the growth time always leads to the increase the tube length as shown in Fig. 4-6. Therefore, we believe that the catalyst role of AAO is minor in the presence of Co catalyst under our experimental conditions.

4.1.4 Field Emission Properties

The field emission current density as a function of electric field for the AAO template based CNTs of three different lengths is shown in Fig. 4-8. It is obvious that the CNTs grown for 30 min (overgrown length: 700 nm-1.5 μm) show better field emission properties than that grown for 15 min (overgrown

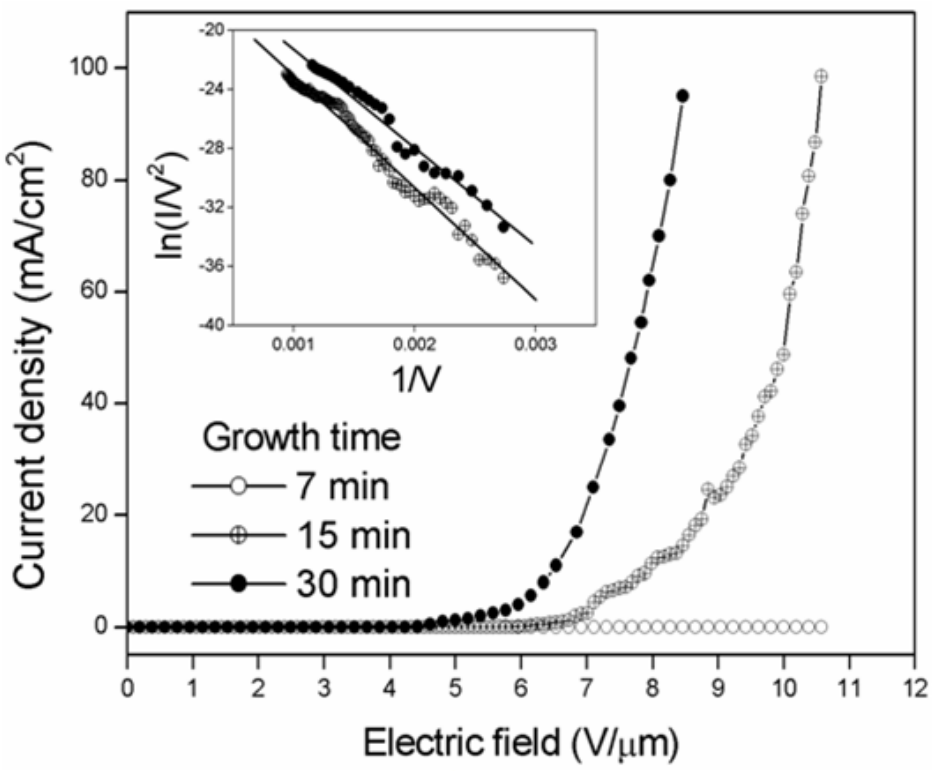

Fig. 4-8. Field emission current density as a function of electric field for the CNTs grown in the AAO nanopores. The inset shows the corresponding Fowler-Nordheim plots.

length: 300-700 nm) and 7 min. The current density of the CNTs grown for 7 min is too low (< 3 μA/cm2) to be observed. The inset in Fig. 4-8 shows the Fowler-Nordheim (FN) plots of the samples. From these plots, we can obtain the field enhancement factor β, which are derived from the slopes by assuming a CNT work function of 5 eV. The β values calculated for the CNTs grown for 30 min and 15 min are 2600 and 1900, respectively. The β values are similar to the values for CNTs grown on an AAO template by Suh et al. [Jung-2002-2392]. It was concluded that the field emission is optimal (β ~ 2650) when the exposed tube

length is similar to the intertube distance, which was about 100 nm in their work. In our experiments, the tube packing density is obviously lower (CNT filled ratio of pores ~ 70%) and results in higher intertube distances. Therefore, the optimal field emission was obtained at an overgrown length above 1 μm. In order to avoid the field screening effect,[Nilsson-2000-2071] a lower packing density of CNTs is favorable.

4.1.5 Summary

In the experiment, we have synthesized vertically aligned CNT arrays, in terms of the AAO templation, by microwave plasma ECR-CVD. Both the AAO template effect and the DC bias as well as the plasma induced self-bias contribute to the vertical alignment of the tubes. The obtained CNT arrays have a very high packing density (as high as ~ 6×10^9 tubes/cm^2) and a narrow diameter distribution (about 75 nm), which are in accordance with the pore arrays of AAO template. The tube growth was catalyzed by the pre-deposited Co catalyst inside the nanopores rather than the AAO template, and the tubes encapsulate Co particles at their tips suggesting the tip growth mechanism. These CNTs are multi-walled and well-graphitized and have good field emission properties. They have potential applications for cold-cathode flat panel displays.

4.2 Tube number density control of CNTs in AAO

4.2.1 Mechanisms of density control

Figures 4-9(a)-(c) show the side-view SEM images of the AAO assisted CNTs grown at CH_4 concentrations of 9%, 50%, and 91%, respectively. As shown, the CNT density changes dramatically relying on the carbonaceous gas content. At 9% CH_4 concentration [Fig. 4-9(a)], the tube number density of CNT is as high as 9.0×10^9 tubes/cm^2 implying a tube filled ratio in pores of about 82%. In an extremely high CH_4 concentration of 91% [Fig. 4-9(c)], the observed tube number density decreases significantly to about 2.0×10^9 tubes/cm^2 (corresponding tube filled ratio of about 18%). These figures also reveal that the nanotubes are uniform in diameter and tend to vertically aligned. Figure 4-10 is a high-resolution transmission electron microscopy (HRTEM) image of CNT shown in Figure 4-9(b). Because the tube has a relatively large diameter, only a part of the tube is shown in this figure. The multi-walled tube is composed of about 70-80 well-ordered graphitic walls and a 7-nm-wide hollow core. The inset in Figure 4-10 shows that a Co catalyst particle is encapsulated at the tip of tube and covered by graphitic cap, suggesting that the CNT is Co-catalyzed and can be divided into the tip-growth mechanism.[Baker-1989-315]

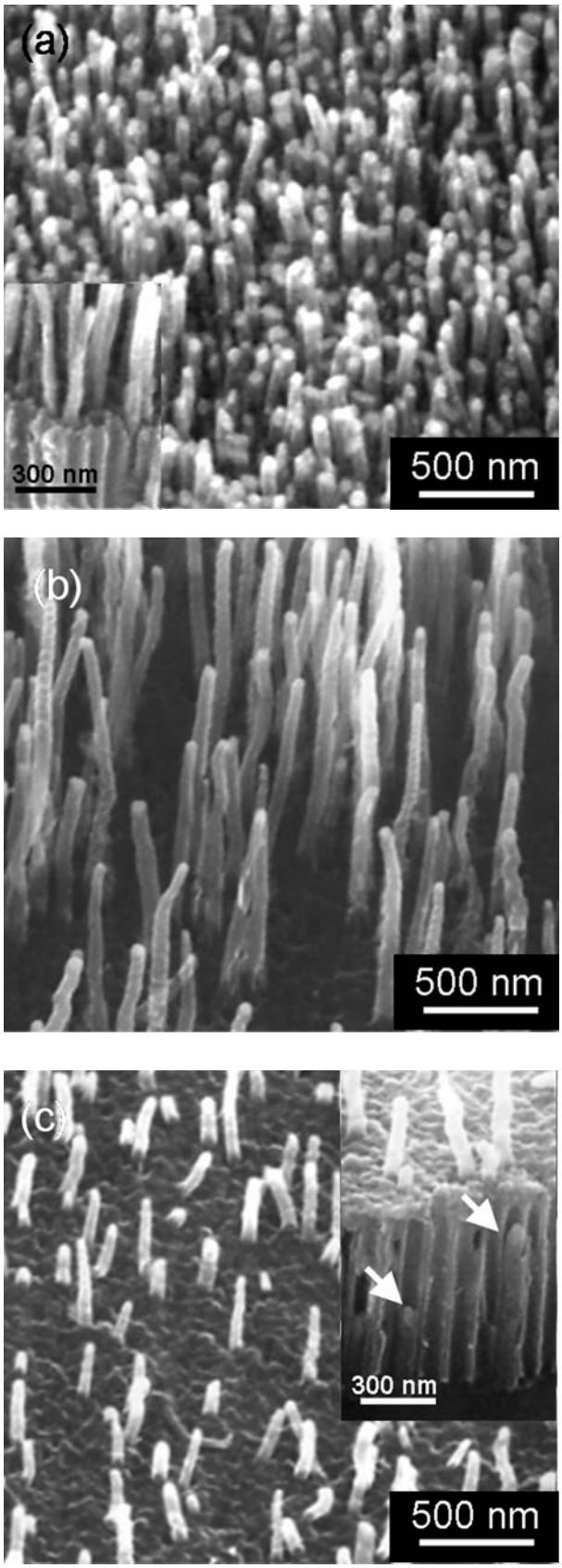

Figure 4-9. (a), (b), and (c) are the side-view SEM images of the AAO assisted CNTs grown at CH_4 concentrations of 9%, 50%, and 91%, respectively. The in-sets in (a) and (c) are the cross-sectional view of the AAO assisted CNTs.

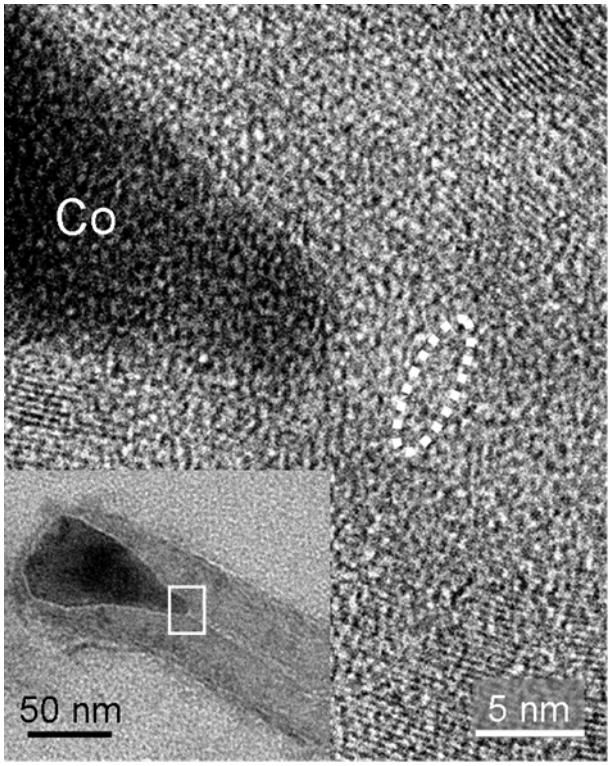

Fig. 4-10 HRTEM image of a Co-catalyzed CNT shown in Figure 4-9(b). The hollow core is indicated by a dashed ellipse. The inset is a corresponding low magnification TEM image. The square presents the magnified area of the HRTEM image.

The growth of CNTs in AAO template is crucially affected by the CH_4/H_2 ratio of precursor gas. Figure 4-11 plots the tube number density and the over-grown tube length of the CNTs as a function of the CH_4 or H_2 concentration. It is seen that not only the tube density decreases linearly with increasing CH_4 concentration/decreasing H_2 concentration, but the tube length decreases as well especially at high CH_4 content. We believe that these phenomena correlate closely with the roles of H_2 during the CNT growth in a CH_4/H_2 plasma. It is

well known that H_2 content in plasma has a strong etching effect on the growing carbonaceous film and promotes the decomposition of CH_4 gases.[Olivier-1998-2113, Young-2000-1864] During the CNT growth, carbonaceous reactive species (such as CH_4 radicals) are generated by hydrogen abstraction reactions[Thanh-1994-8014] and then decomposed by catalyst assistance. These reactive species will eventually initiate the formation of CNTs. A large content of H_2 in plasma can effectively decompose the CH_4 gas, resulting in a large amount of reactive species and thus a high growth rate of CNTs. Therefore, in our results, the tube length was shortened significantly following the increase of the CH_4/H_2 feed ratio [Fig. 4-11(b)], which is essentially a consequence of decreasing the CH_4 pyrolysis efficiency. When the CH_4 concentrations are below 50%, however, the obtained tube lengths are very close. This is due to that after the CNTs grown to these lengths the Co catalyst had been poisoned. Even if the growth time was increased further, the nanotubes did not grow anymore.

It was reported that while the Co-catalyzed CNTs was grown on AAO template, the nanotube growth and the carbon deposition on AAO pore wall take place simultaneously.[Jeong-2002-4003] As shown in Figure 4-9(c), the AAO surface was covered with a thin layer of carbonaceous sediment which blocks the outgrowth of most CNTs. In order to investigate the nature of carbon in the CNT and on the AAO surface, Auger electron spectroscopy (AES) analyses were con-

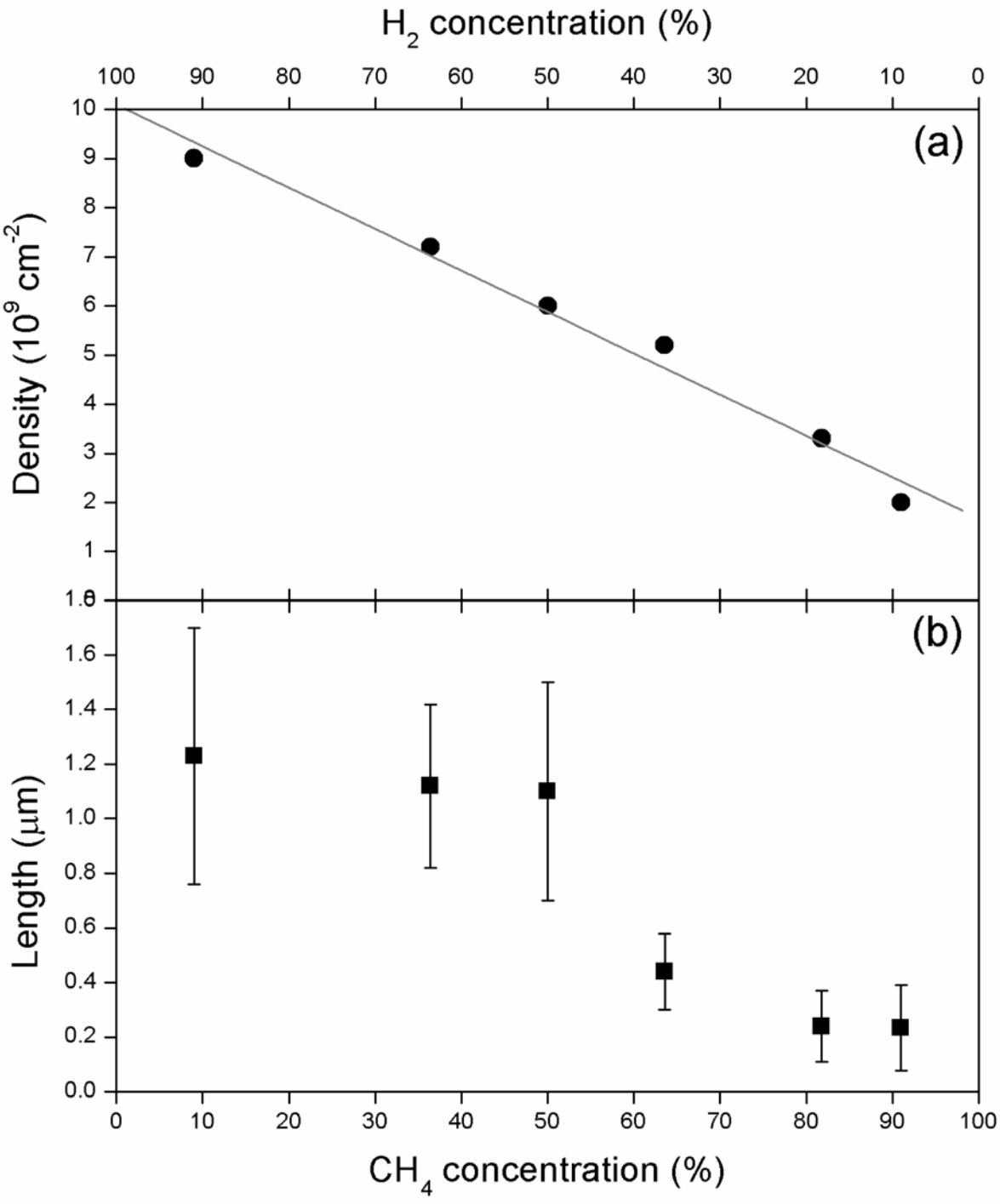

Fig. 4-11. (a) Tube number density and (b) overgrown tube length of the AAO assisted CNTs as a function of the CH_4 or H_2 concentration.

ducted using a VG Microlab 310F Auger Nanoprobe system with Schottky field emission electron source. Figure 4-12 shows the Auger carbon (*KVV*) signals of a commercially single-walled CNT (SWCNT) (for comparison), an AAO assisted CNT, and the carbonaceous films on AAO surface. By line shape analysis of the Auger carbon transition, one can obtain the qualitative insight on the bonding of the carbon atoms in different carbon-based materials, such as diamond, graphite, and amorphous carbon.[Lurie-1977-476, Teo-2002-116] The peak features present that the carbon of CNT produced in this study as well as commercial SWCNT is predominantly well-crystallized sp^2-bonded (crystalline graphite-like). As for the carbonaceous films on AAO surface, the KV_2V_3 troughs situated near 258 eV decay obviously, suggesting that the films mainly consist of amorphous sp^2 carbon. Moreover, the Auger carbon peak of the carbonaceous film grown at 50% CH_4 concentration is much smoother than that grown at 91% CH_4. This indicates that the phenomenon of amorphous carbon deposition is weaker under the growth conditions of lower CH_4 concentration.

During the CNT growth, the amorphous carbon byproduct is simultaneously deposited and further etched away by H^+ species in the plasma. If a high CH_4/H_2 feed ratio is used, the amorphous carbon deposition predominates over the etching action, resulting in the continuing growth of amorphous carbon. In this study, the generally undesired amorphous carbon was employed to control

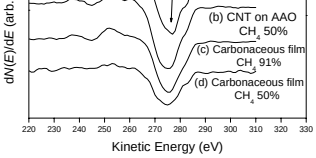

the tube number density of CNTs on AAO template. Because the CNT growth and the amorphous carbon deposition proceed simultaneously, there is a competition reaction between them. In a high CH_4/H_2 feed ratio, a high amorphous carbon deposition rate is appeared, and furthermore the CNT growth rate is rather low [Figure 4-11(b)]. These double effects cause a consequence of that most nanotubes were blocked inside the AAO nanopores by the amorphous carbon layer and were unable to grow out. As indicated in the inset of Figure 4-9(c), some short nanotubes marked by white arrows were buried inside the nanopores without growing out. Conversely, in a low CH_4/H_2 feed ratio, the AAO surface

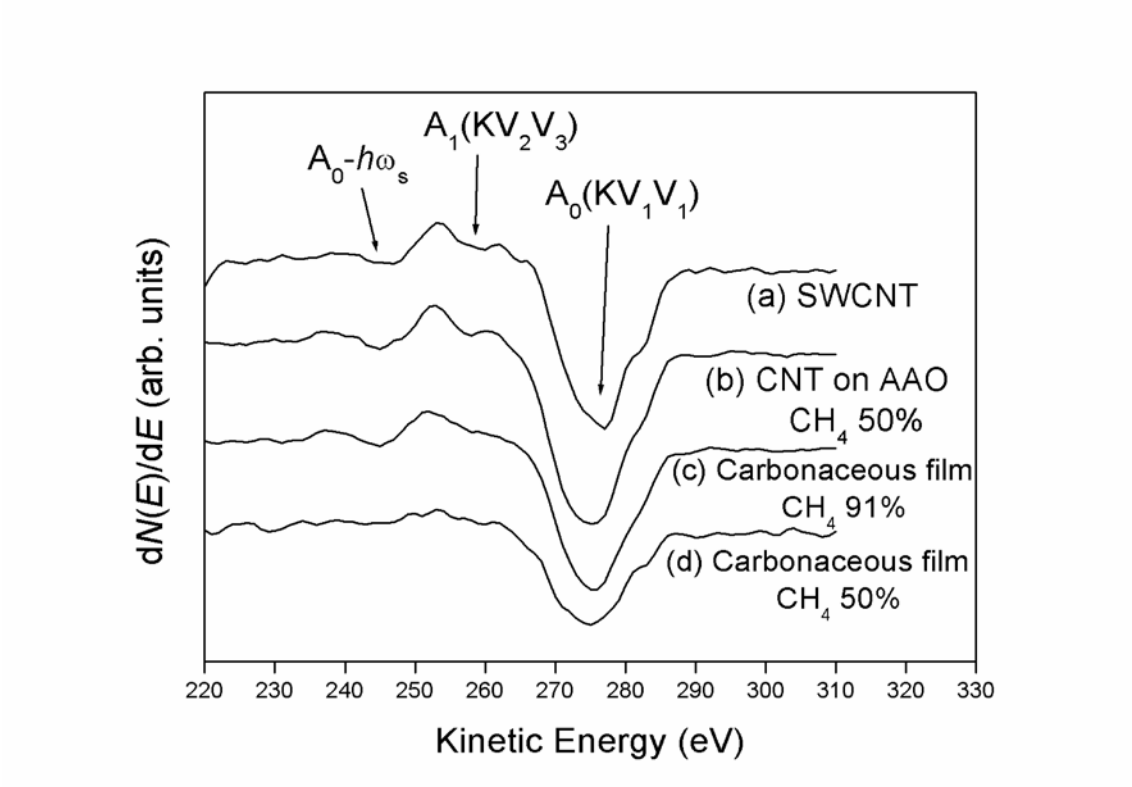

Figure 4-12. Graphitic Auger carbon (*KLL*) peaks of (a) a commercially single-walled CNT, (b) an AAO assisted CNT grown at 50% CH_4, (c) the carbonaceous film on AAO surface grown at 91% CH_4, and (d) 50% CH_4.

will free from amorphous carbon as it is etched away by H^+ species [the inset in Figure 4-9(a)], and CNTs grow fast, leading to an ultra high tube number density. In this context, the number of CNTs escaped from the AAO nanopores is strongly influenced by the CH_4/H_2 feed ratio. As shown in Figure 4-11(a), there is a linearly inverse proportional relationship between the tube density and the CH_4 concentration.

4.2.2 Raman Spectrum Analysis

Raman spectra of the vary samples of Figures 4-9(a)-(c) are presented in Figure 4-13. The spectra excited with the 632.8 nm line of a He-Ne laser show mainly two bands located at 1330 cm^{-1} (*D* band) and 1590 cm^{-1} (*G* band). The *G* band indicates the presence of crystalline graphitic carbon in the multi-walled CNTs, and the *D* band originates from defects in the graphite and finite particle size effect.[Tuinstra-1970-1126] With regard to the CNTs produced in this study, however, the *D* band is stronger than the *G* band, implying that the nanotubes are possessed of an un-neglected defect density. Moreover, the Raman signal of the CNTs grown at 91% CH_4 concentration is more intense compared with that grown at 50% and 9% CH_4. This may due to that the large amounts of amorphous carbon on AAO surface also contributes to the Raman signal. We conclude that the high defect density of CNTs is most possibly related to the serious

ion bombardment effect in the ECR plasma environment. Because of the low working pressure of ECR plasma (0.25 Pa), there is a considerably long mean-free path (MFP) of CH_4 molecule evaluated as about 38.1 cm under the plasma condition, and therefore a high kinetic energy of ionized species (CH_4^+ or CH_3^+)[Shiratori-2003-2485] can be obtained. These high speed cations are accelerated by -150 V substrate bias and plasma sheath potential, and finally fly to collide the growing CNTs, leading to lattice distortion or *c*-axis stacking disorder of graphitic walls.

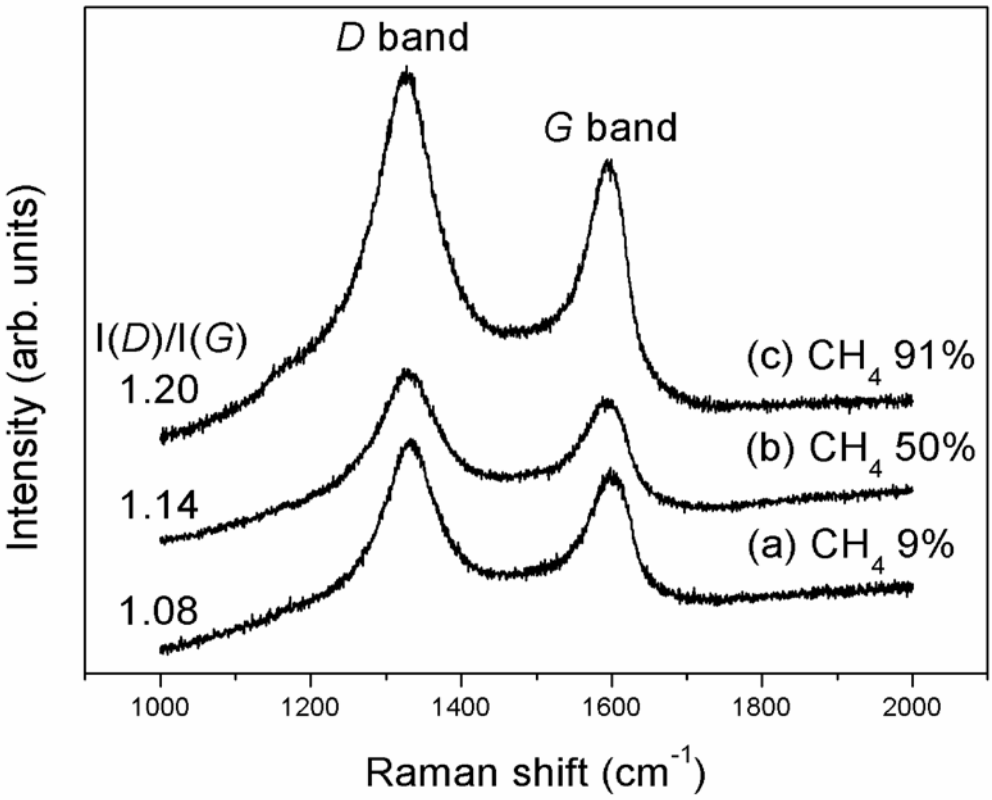

Figure 4-13. Raman spectra of the AAO assisted CNTs grown at (a) 9% CH_4, (b) 50% CH_4, and (c) 91% CH_4.

4.2.3 Field Emission Measurement

Figure 4-14 shows the field emission current density as a function of applied electric field, measured from the AAO template based CNTs with three different tube number densities shown in Figures 4-9(a)-(c). Measurements were conducted by the simple diode configuration [Fig. 3-3] and performed in a high vacuum chamber (about 10^{-6} torr). The distance between the CNTs and anode was about 100 μm. Because of a serious field-screening effect, the CNT array with an ultra-high density of 9.0×10^{9} tubes/cm^2 shows the worst emission properties in terms of the highest turn-on electric field (E_{to}) of 8.1 V/μm and the lowest current density, in which E_{to} is here defined as electric field required for the emission current density of 1 mA/cm^2. As the tube density was decreased to about 6.0×10^{9} tubes/cm^2, the field emission properties remarkably improved (E_{to} ～ 5.2 V/μm) due to an enhanced electric field. However, the field emission properties deteriorated once more (E_{to} ～ 7.4 V/μm) in the event that further decreased the tube density to about 2.0×10^{9} tubes/cm^2. Such field emission deterioration of CNTs is probably caused by the amorphous carbon layers on the tube surface left during the CNT growth at a high CH_4 concentration. In a growth condition of high CH_4 concentration, the amorphous carbon layers are deposited on not only AAO surface but CNT surface. The amorphous carbon on

CNT surface would generate an energy barrier and thus reduce the emitted current.[Gao-2003-5602] Figure 4-15 presents the corresponding Fowler-Nordheim (FN) plots of the data shown in Figure 4-14. The enhancement factors β are derived from the slopes of the FN plots by assuming a CNT work function of 5 eV. It is obvious that only the FN plot of CNTs grown at high CH_4 concentration of 91% shows two linear segments with different slopes attributed to the amorphous carbon induced energy barrier. At a high electric field region (> 7.7 V/μm), the slope of the FN plot was noticeably decreased and the β value was increased from about 1141 to 3132, suggesting that the energy barrier was overcome and thus more electrons could be emitted. In contrast, the FN plots of CNTs grown at 50% and 9% CH_4 concentrations mainly show only one β value of about 2597 and 1154, respectively, due to a relatively clean CNT surface. Although the amorphous carbon can effectively decrease the tube number density of CNTs on AAO, such impurity would interference the electron emitting from CNTs. Nevertheless, it is expected that if only the CNT surface is cleaned up by post-growth treatment, such as H_2 plasma treatment, the low tube density provided field enhancement will be more highlighted.

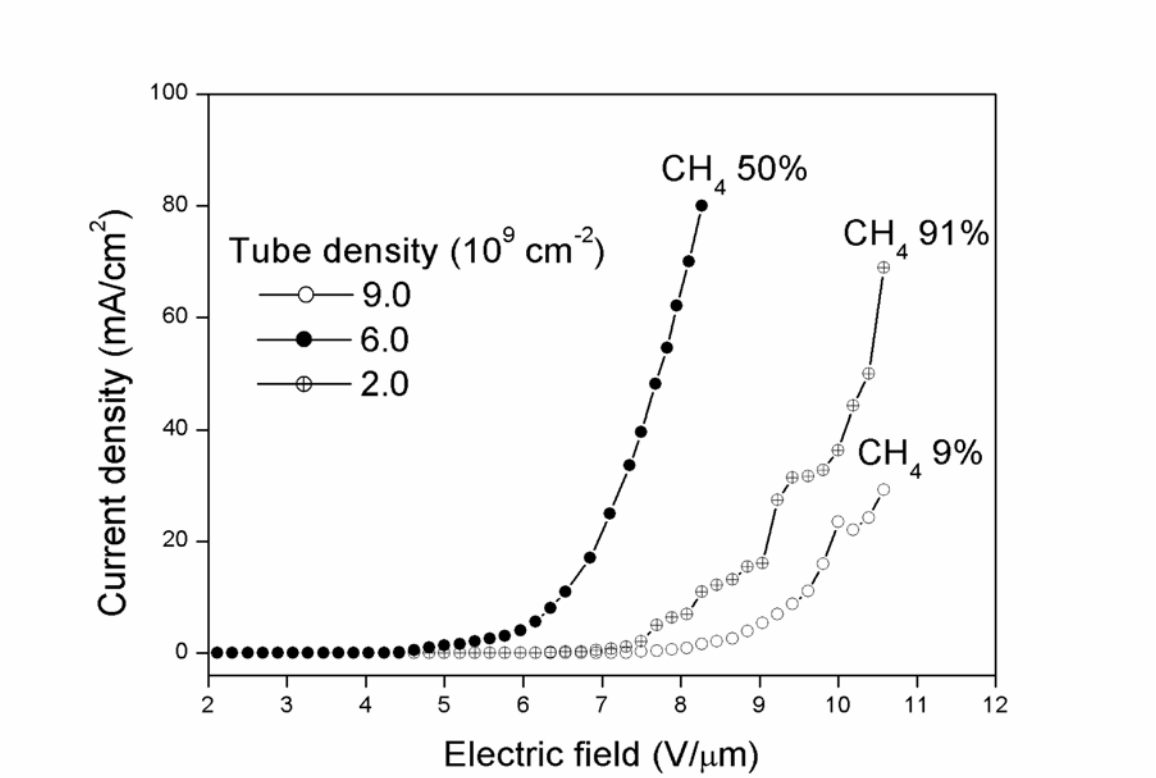

Figure 4-14. Field emission current density as a function of electric field for the CNTs grown on the AAO template with three different tube number densities shown in Figures 4-9(a)-(c).

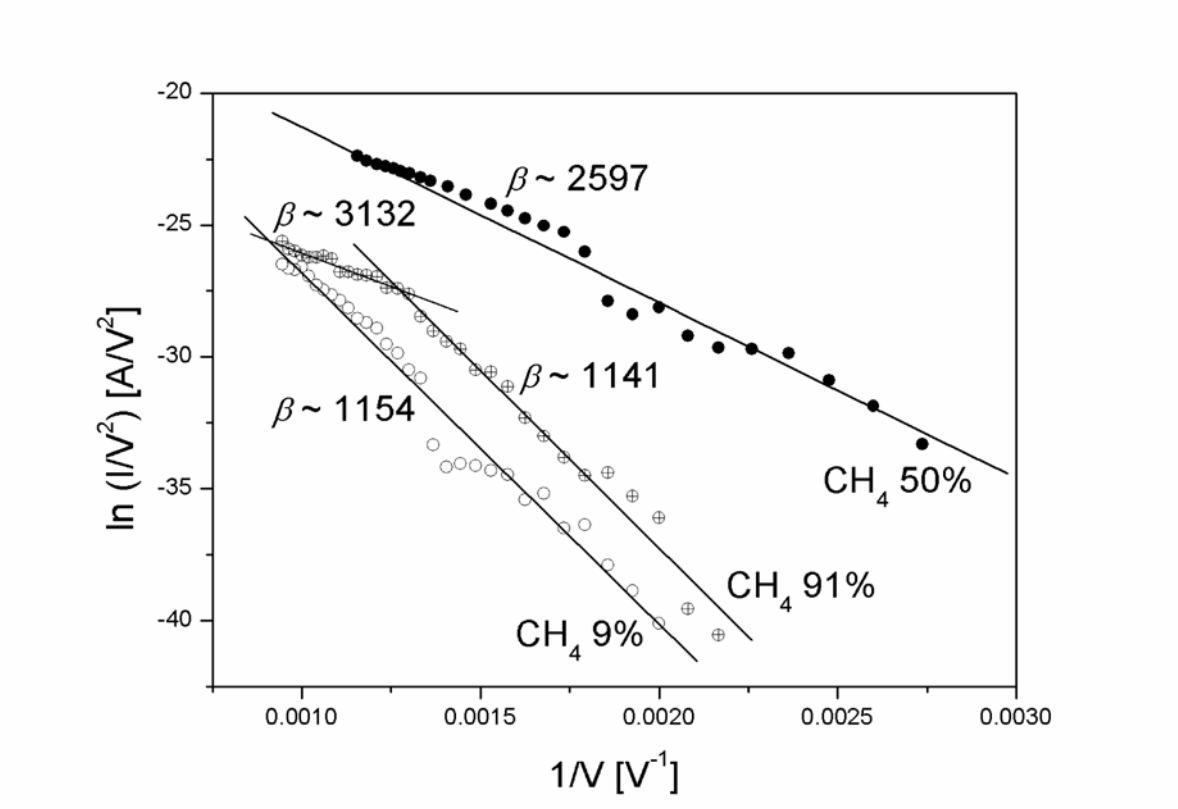

Figure 4-15. Corresponding Fowler-Nordheim plots of the data shown in Figure 4-14.

4.2.4 Summary

In summary, tube number density of AAO template assisted CNTs can be controlled by *in situ* regulating the flow rate ratio of CH_4/H_2 precursor gases. Following the increase of the CH_4 concentration, the tube number density and tube length decrease significantly. In a low CH_4/H_2 feed ratio, the AAO surface was free from amorphous carbon as it is etched away by H^+ species, and CNTs grow fast, resulting in an ultra high tube density. In the case of the high CH_4/H_2 feed ratio, the amorphous carbon was continually deposited on the AAO surface, which blocked the CNT outgrowth, and therefore lowered the tube density. Enhanced emission properties were achieved by lowering the tube density. However, an excessively high CH_4/H_2 feed ratio would lead to an amorphous carbon induced energy barrier and thus deteriorate the electron emitting. It was found that the field emission was optimal in a moderate tube density of about 6.0×10^9 tubes/cm^2.